HARD X-RAY MICROFLARES DOWN TO 3 keV

SÄM KRUCKER[1], STEVEN CHRISTE[1] , R. P. LIN[1,2], GORDON J. HURFORD[1] and RICHARD A. SCHWARTZ[3]
[1]*Space Sciences Lab, University of California, Berkeley, CA 94720-7450, U.S.A.*
[2]*Physics Department, University of California, Berkeley, CA 94720-7450, U.S.A.*
[3]*SSAI & Laboratory for Astronomy and Solar Physics, NASA Goddard Space Flight Center, Greenbelt, MD 20771, U.S.A.*

(Received 7 August 2002; accepted 17 September 2002)

Abstract. The excellent sensitivity, spectral and spatial resolution, and energy coverage down to 3 keV provided by the Reuven Ramaty High-Energy Solar Spectroscopic Imager mission (RHESSI) allows for the first time the detailed study of the locations and the spectra of solar microflares down to 3 keV. During a one-hour quiet interval (GOES soft X-ray level around B6) on 2 May, 1:40–2:40 UT, at least 7 microflares occurred with the largest peaking at A6 GOES level. The microflares are found to come from 4 different active regions including one behind the west limb. At $7''$ resolution, some events show elongated sources, while others are unresolved point sources. In the impulsive phase of the microflares, the spectra can generally be fitted better with a thermal model plus power law above ~ 6–7 keV than with a thermal only. The decay phase sometimes can be fitted with a thermal only, but in some events, power-law emission is detected late in the event indicating particle acceleration after the thermal peak of the event. The behind-the-limb microflare shows thermal emissions only, suggesting that the non-thermal power law emission originates lower, in footpoints that are occulted. The power-law fits extend to below 7 keV with exponents between -5 and -8, and imply a total non-thermal electron energy content between 10^{26}–10^{27} erg. Except for the fact that the power-law indices are steeper than what is generally found in regular flares, the investigated microflares show characteristics similar to large flares. Since the total energy in non-thermal electrons is very sensitive to the value of the power law and the energy cutoff, these observations will give us better estimates of the total energy input into the corona. (Note that color versions of figures are on the accompanying CD-ROM.)

1. Introduction

The Reuven Ramaty High-Energy Solar Spectroscopic Imager (RHESSI) instrument (see Lin *et al.*, 2002) provides uniquely high sensitivity in the energy range from ~ 3 to 15 keV, together with ~ 1 keV FWHM spectral resolution and simultaneously imaging down to 2.3 arc sec. This energy range covers emissions from hot, ≥ 5 MK thermal plasmas and from accelerated, non-thermal low-energy electrons. Previous solar hard X-ray instruments, such as HXRBS flown on SMM and HXT on *Yohkoh*, have entrance windows that absorb emission below ~ 15–25 keV to avoid saturation from the intense thermal emissions in large flares (Kane and Anderson, 1970). For balloon-borne instruments (Lin *et al.*, 1984), the Earth's atmosphere absorbs solar hard X-rays below ~ 15 keV. The RHESSI instrument

Solar Physics **210:** 445–456, 2002.
© 2003 *Kluwer Academic Publishers. Printed in the Netherlands.*

accommodates medium and large flares by automatically inserting shutters in front of detectors to absorb low-energy photons and avoid saturation. Instruments designed to measure solar flare soft X-rays generally have very small effective areas above ~ 3 keV. The instrument most comparable to RHESSI in this energy range, the Hard X-ray Imaging Spectrometer (HXIS) on the *Solar Maximum Mission*, provides effective areas of ~ 0.7 mm^2 at ~ 3.5 keV rising to ~ 7–26 mm^2 at ~ 10 –15 keV (Van Beek *et al.*, 1980). For comparison RHESSI, with shutters out, has an effective area of ~ 10 mm^2 at ~ 3.5 keV, rising rapidly to ~ 250 mm^2 at 5 keV and ~ 3500 mm^2 at 10–15 keV; a factor of ~ 14 to ≥ 130 times larger. Thus, the RHESSI observations from ~ 3 to 15 keV with the shutters out can provide new information on low-level energy releases, whether they result in heating of hot thermal plasmas or in the acceleration of low-energy electrons.

It is evident from previous observations that the Sun releases energy in transient outbursts, ranging from major flares ($\sim 10^{32}$–10^{33} ergs) down to microflares and even nanoflares, with the frequency of the releases increasing as the energy released decreases (see discussion in Aschwanden *et al.*, 2000). For flares, the energy releases often appear to be dominated by accelerated ~ 10s of keV electrons and sometimes ~ 1 MeV nucl^{-1} ions. Hard (> 20 keV) X-ray microflares, tiny bursts with $\sim 10^{27}$ to 10^{28} ergs in > 20-keV electrons, were discovered with a balloon-borne instrumentation to occur on average once every ~ 6 min near solar maximum (Lin *et al.*, 1984), leading to speculation that the energy released in accelerated electrons, summed over HXR bursts of all sizes, might contribute significantly to the heating of the active corona.

Lin, Feffer, and Schwartz (2001) investigated HXR microflares at lower energies using the BATSE SPEC detectors on the Compton Gamma-Ray Observatory, whose thresholds were occasionally set as low as 8 keV. They found that only one third of all non-thermal (hard spectra unlikely to be thermal) events detected above 8 keV are observed above ~ 25 keV. Additionally, the generally steep HXR spectra (power-law fits with exponent of 3–7) reveal that most of the flare energy is in the non-thermal electrons at lowest energy. Furthermore, the similarity of frequency vs. energy release distribution of these > 8 keV bursts to that of active-region transient brightenings (ARTBs) seen in soft X-rays by the *Yohkoh* SXT instrument (Shimizu, 1995) suggests that these accelerated electrons may provide the energy for ARTBs. Here, the first RHESSI spectra and images of microflares detected above 3 keV are presented and discussed.

2. Data Analysis

Standard RHESSI software (Hurford *et al.*, 2002) was used to analyze data. First, GOES and RHESSI data were searched for times with low solar activity when both shutters were out; the shutters (Lin *et al.*, 2002) suppress the response below 10 keV by a factor of 50 or more. Then, the microflares were identified and a

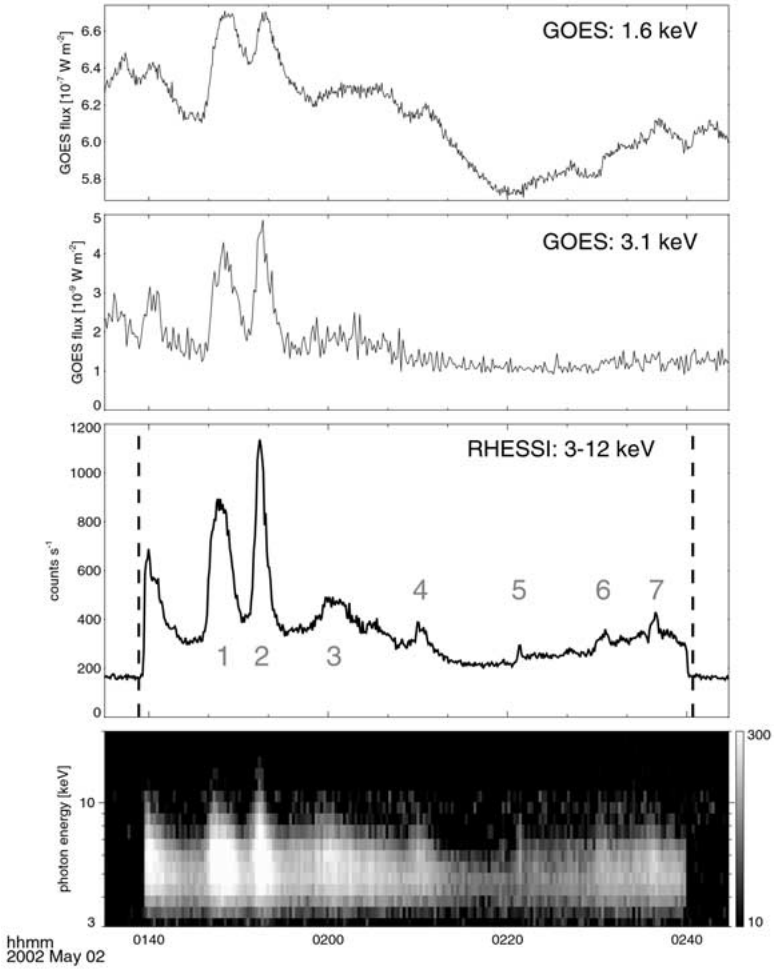

Figure 1. RHESSI and GOES X-ray observations during times of low solar activity. Around one hour of observations are shown corresponding to one RHESSI day. The *vertical dashed lines* give the sunrise and sunset, respectively. *From top to bottom*: softer and harder GOES channel plotted in a linear scale, the RHESSI X-ray total uncalibrated counts between 3 and 12 keV, and the RHESSI count spectrogram plot (background subtracted). The microflares studied in detail are marked with numbers (for color version of figures see the accompanying CD-ROM).

full disk image of each microflare was made with a resolution of $\sim 60''$ to obtain the centroid position. In a second step, cleaned images of each microflare around the flare position are made using higher resolution. Since grid 2 (4 arc sec) has a ~ 20 keV threshold, these images are reconstructed with $7''$ resolution (grid 3). Initial imaging with the finest resolution (2.3 arc sec) by grid 1 did not improve the image, suggesting no structures at the $2''$ level. However, more analysis is needed.

The spectra shown here are produced using the SPEX software package. Energy bins corresponding to the FWHM resolution of 1 keV are used. The relatively low

number of counts and the absence of a wide range in energy where non-background counts are detected make fitting of the microflare spectra challenging. Microflares are typically seen from 3 keV up to 15 keV, giving 12 data points to fit. Additional complications are given by the iron line at 6.7 keV (cf., Tanaka *et al.*, 1984) that are ignored in this preliminary study. Furthermore, the fitted parameters depend on the background subtractions. Generally, the total pre-event background – instrumental, non-solar, and solar background – are subtracted before fitting the spectra. This is appropriate if the pre-event contribution of the flaring source can be neglected, but inappropriate if the flaring loop is already contributing significantly to the pre-event emission. One way to distinguish these two scenarios is to image the pre-event emission. If the pre-event emission is coming from a different location than the flare site, then the total pre-event background should be subtracted. If not, subtracting the background spectra observed during RHESSI night might give better results. The background subtractions used in this paper are still preliminary and more investigations are needed (see also discussion in Benz and Grigis 2002). The spectra shown in Figure 4 are obtained by subtracting the night time background for microflares 1 and 2 and the pre-event background for microflare 3.

Two models were fitted to the derived spectra and compared: (a) a thermal fit only, (b) a thermal fit plus a non-thermal power law. (For a discussion on a double thermal model see Benz and Grigis (2002, this issue.) The thermal fit contains only two parameters, temperature and emission measure; the thermal plus non-thermal fit has three more parameters: the power law exponent, the low energy cutoff below which the non-thermal spectrum is assumed flat, and the intensity. There are clear cases when a thermal alone does not fit the data at all, as often observed in the rise phase of an event; or when the thermal alone already fits the data well enough. The less clear cases are when the thermal fit gives only moderate agreement with the data and an additional non-thermal fit provides smaller residuals; but often the derived power law index is very steep with values around 10.

The derived power-law exponent is reasonably accurate, giving consistent values within ± 0.5, even when using different values for the subtracted background. At lower energies where the thermal is fitted, the uncertainties are introduced mostly by the selection of the background as described above. At energies above ~ 10 keV, the component of the pre-event solar background is smaller than the non-solar background and the selection of the solar background is less critical. Therefore, the derived values for the temperature and emission measure from the thermal fit are more uncertain and still preliminary. The accuracy of the derived temperatures is estimated to ± 2 MK from multiple fitting of the same events with different background subtractions and different initial guesses of parameters. Subtracting the solar pre-event background gives generally higher temperatures (up to ~ 2 MK) than subtracting the background observed during night. The accuracy of the logarithm of the emission measure is around ± 0.5 and is inversely correlated to the error in temperature. For the largest microflares that produce a clear enhancement in both GOES channels, independent temperature estimates can be derived

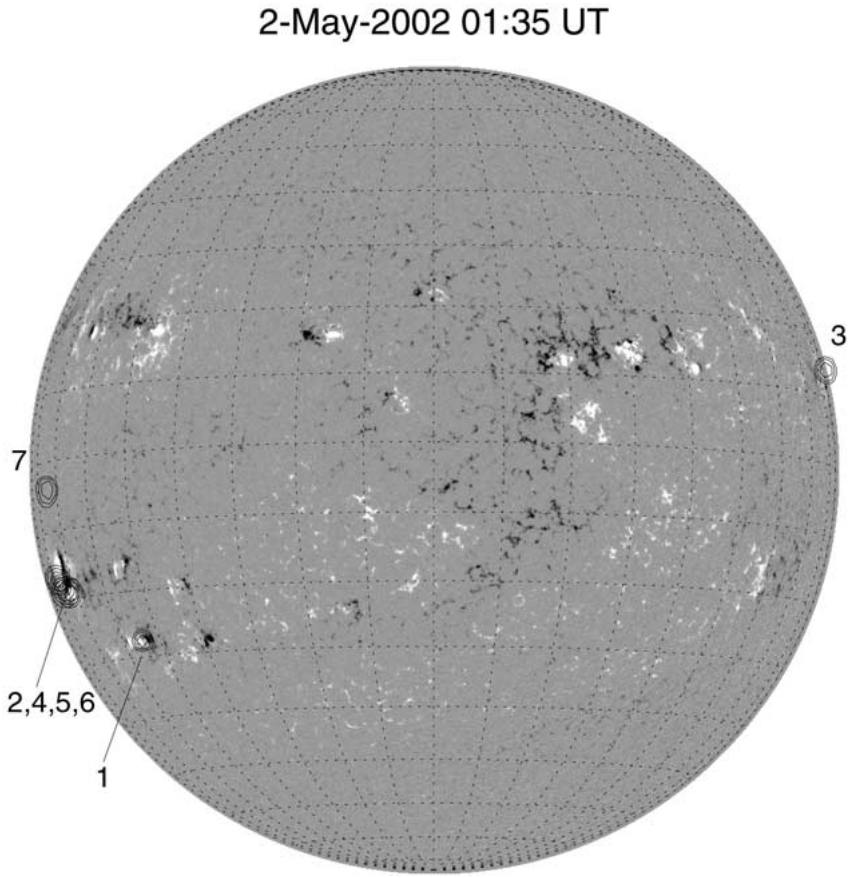

Figure 2. The locations of the 7 microflares marked in Figure 1 are shown on an MDI magnetogram.

using the ratio of the two GOES channels. The derived temperatures from GOES are generally smaller but roughly consistent within the error estimates given above.

3. Observations

One orbit of RHESSI data is shown here as an example of microflare activity seen down to 3 keV (Figure 1). The time period selected is 2 May 2002, 01:40–02:40 UT, with a GOES soft X-ray background level around B6. The same time interval is also discussed by Benz and Grigis (2002). During this period, at least 7 microflares could be easily identified (marked with numbers in Figure 1). A number of even smaller transient increases – e.g., at 02:04, 02:19, 02:27, 02:32, and 02:36 UT – appear to be significant in the 3–12 keV count rates. After subtracting the GOES background flux, the largest microflare has a peak GOES soft X-ray classification of A6, while the smallest of the 7 microflares is around A0.1,

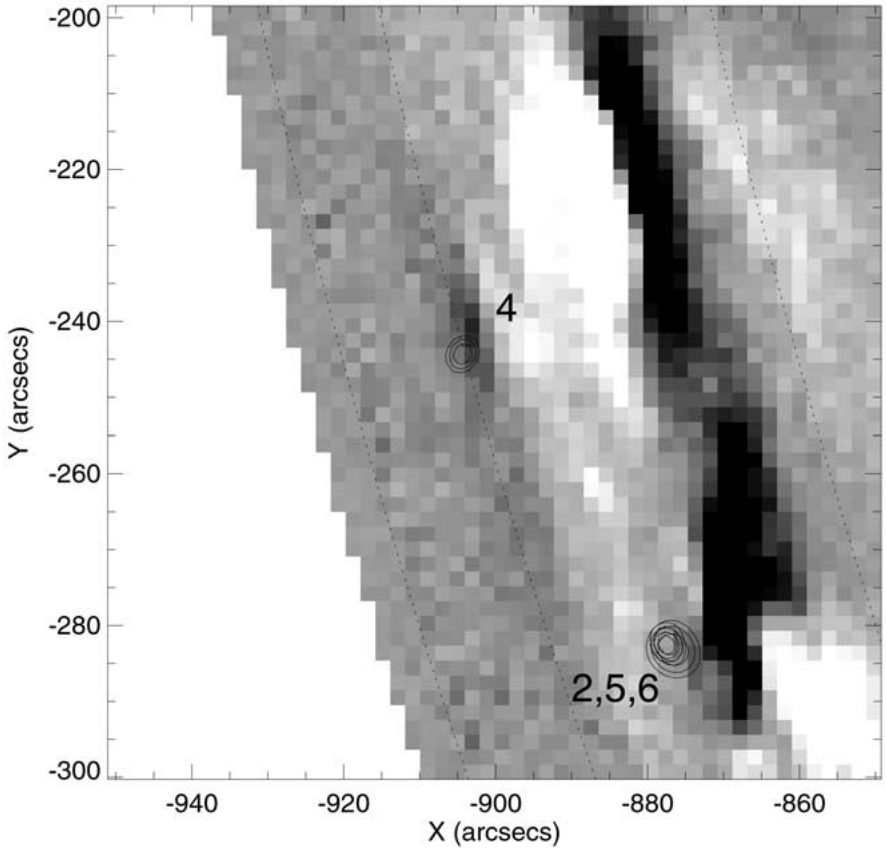

Figure 3. Zoom of Figure 2 showing the 4 microflares occurring in AR 9934 with 7″ resolution.

hardly detectable above the GOES background. Compared to the GOES survey of flare sizes reported by Feldman *et al.* (1996), the largest microflare presented here corresponds to the smallest flares presented in their study.

3.1. MICROFLARE IMAGING

Figure 2 shows cleaned images of the microflares numbered in Figure 1 superimposed on a full-disk MDI magnetogram. All the HXR microflares analyzed so far are found to originate from active regions. The 7 microflares outlined in Figure 1 come from 4 different active regions: microflare 1 is from the southeast (NOAA AR 9932), microflares 2,4,5,6 from the nearby active region AR 9934, microflare 3 originates from just behind the limb (AR 9915), and microflare 7 occurs in a newly emerging active region near the east limb (AR 9938). Imaging at 7″ resolution show some microflares with elongated sources, while others are spatially not resolved. Figure 3 is an enlarged image of microflares 2, 4, 5, and 6, showing that microflare 4 occurs in a different part of the active region than 2, 5, and 6.

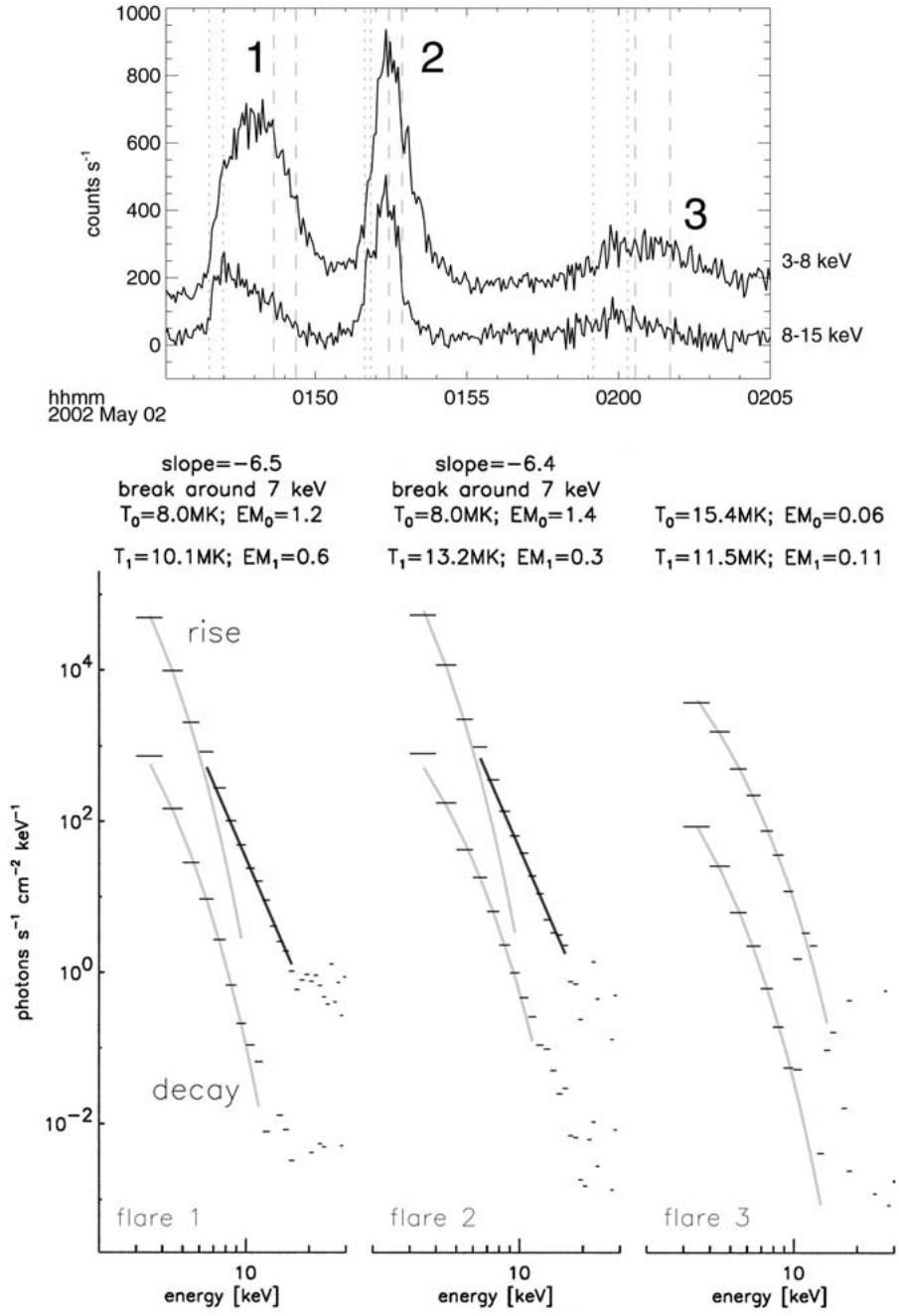

Figure 4. (a) *Top plot* shows the time series of the 3–8 keV and the 8–15 keV energy range that roughly correspond to the thermal and non-thermal energy regime. For a clearer representation, the 8–15 keV time profile is multiplied by a factor of 3. The *gray dotted and dashed lines* give the time intervals used for the fits shown below. (b) Spectra during the impulsive phase (shown shifted up by two decades) and the decay phase of the microflares labeled 1 to 3 in Figure 1. The impulsive phase is fitted with both a thermal and a non-thermal component, the decay phase with a thermal component only. For the behind-the-limb microflare (flare 3), a thermal alone fits the data well enough. The shown curves give the range fitted; values above $\sim$ 15 keV are dominated by noise.

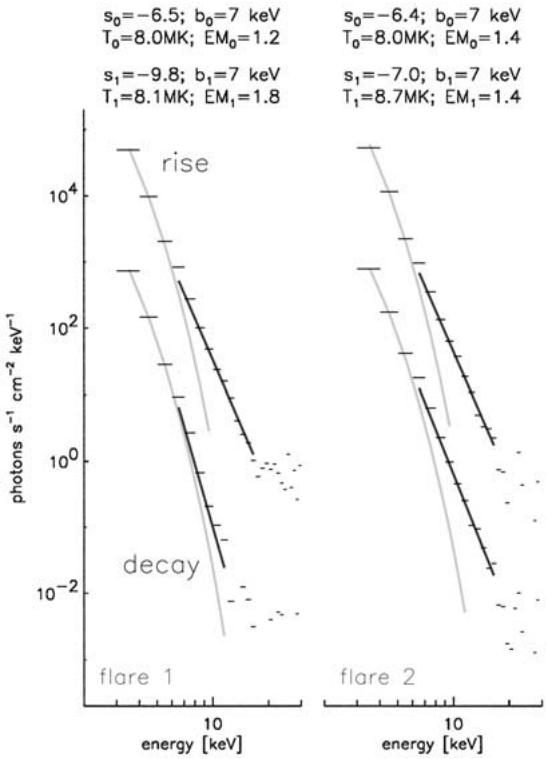

Figure 5. The spectra of microflares 1 and 2 are shown again, but the decay phase is fitted with both a thermal and a non-thermal component.

3.2. MICROFLARE ENERGY SPECTRA

As a preliminary analysis, spectral fits are performed separately to the impulsive phase and the decay phase of the microflares. Examples of spectra of the first three microflares are shown in Figure 3. A thermal fit alone cannot represent the data of microflares 1 and 2 during the impulsive phase, but a thermal plus a non-thermal power-law produces a good fit. The non-thermal power-law fit reveals steep spectra for the 2 May, 01:40–02:40 UT, time interval with exponents ranging from -5 to -8. These are much steeper values than what is generally observed for normal sized flares where the indices are often between -3 and -4, and are somewhat steeper than the > 8 keV microflares (exponents of -3 to -7) reported by Lin, Feffer, and Schwartz (2001). The power laws extend to low energies and the best fit gives low energy cutoffs of around 7 keV for the two biggest microflares with best statistics. The smaller microflare 3 that occurs just behind the limb does not show a clear non-thermal component in the spectra and is best fitted with a thermal spectra only, suggesting that the non-thermal emission is occulted. The fitted temperatures of microflare 3 are rather high compared to the other 6 microflares. Since hotter flares are generally larger flares (e.g., Feldman *et al.*, 1996), this suggests that most

of the microflare emission is occulted and that this microflare might be much larger than the A0.1 level observed by GOES.

The spectra of the decay phases do not show a picture as clear as the impulsive phase. Some events like microflare 1 are moderately well fitted with a thermal emission only, others like microflare 2 are better represented with a thermal plus a non-thermal fit (Figure 5). The thermal fit of microflare 2 alone does not represent the decay phase at 3 keV and above 10 keV (cf., Figure 4). This difference in the spectrum for these two microflares can also be seen in the uncalibrated time profiles above and below 8 keV (Figure 4, top, for calibrated time profiles see Benz and Grigis, 2002): Microflare 1 shows a typical impulsive onset above 8 keV and a more gradual onset at lower energies, reminiscent of the Neupert effect (Neupert, 1968), but for microflare 2, the time profile looks very similar in both energy ranges. Still, the emission below 8 keV has a slightly longer decay phase than above 8 keV. For the decay of microflare 1, the thermal plus non-thermal fit gives a very steep (and therefore questionable) power-law index close to -10, however, it does suggest some non-thermal HXR emission. The thermal fit alone gives a temperature around ~ 8 MK for microflare 1 (Figure 5, left), but does not fit the emission at 3 keV or above 10 keV well.

3.3. Microflare seen in RHESSI and TRACE

To place these HXR microflares in the context of lower temperature flare emission, a microflare occurring on 6 May 2002, 09:01 UT (Figure 6), which is comparable to the largest flare occurring in the 2 May time interval (GOES A8 level), is presented here. The RHESSI time profiles above and below 8 keV show two peaks about 2 minutes apart with the first peak harder than the second one. No TRACE overlap is available for the 2 May time interval except for the behind limb flare that did not show any enhanced emission in EUV (195 Å).

The 6 May microflare is compared with TRACE images in four different phases: (1) pre-flare phase, (2) rise to first peak, (3) main (second) peak, and (4) late in the decay phase. In EUV (195 Å) this event shows two bright spots flaring that are already visible in the pre-flare image. These 195 Å sources show a very similar time profile as in X-rays; with two peaks as well. The X-ray emission below 8 keV occurs between the two EUV spots, suggesting a hot loop in between. Above 8 keV, the X-ray image looks different with a strong source near the western EUV spot and a possible weaker source possibly related to the eastern EUV spot. The image above 8 keV is reconstructed with relatively low statistics and therefore is of lower quality. Still, the rise phase of this microflare can be interpreted as a single loop brightening with footpoints seen above 8 keV and the loop top seen at lower energies.

During the main peak of the event, the emission below and above 8 keV comes only from the loop. About 8 minutes after the rise phase, a very fine and slightly curved loop is seen with TRACE connecting the earlier flaring footpoints. The X-

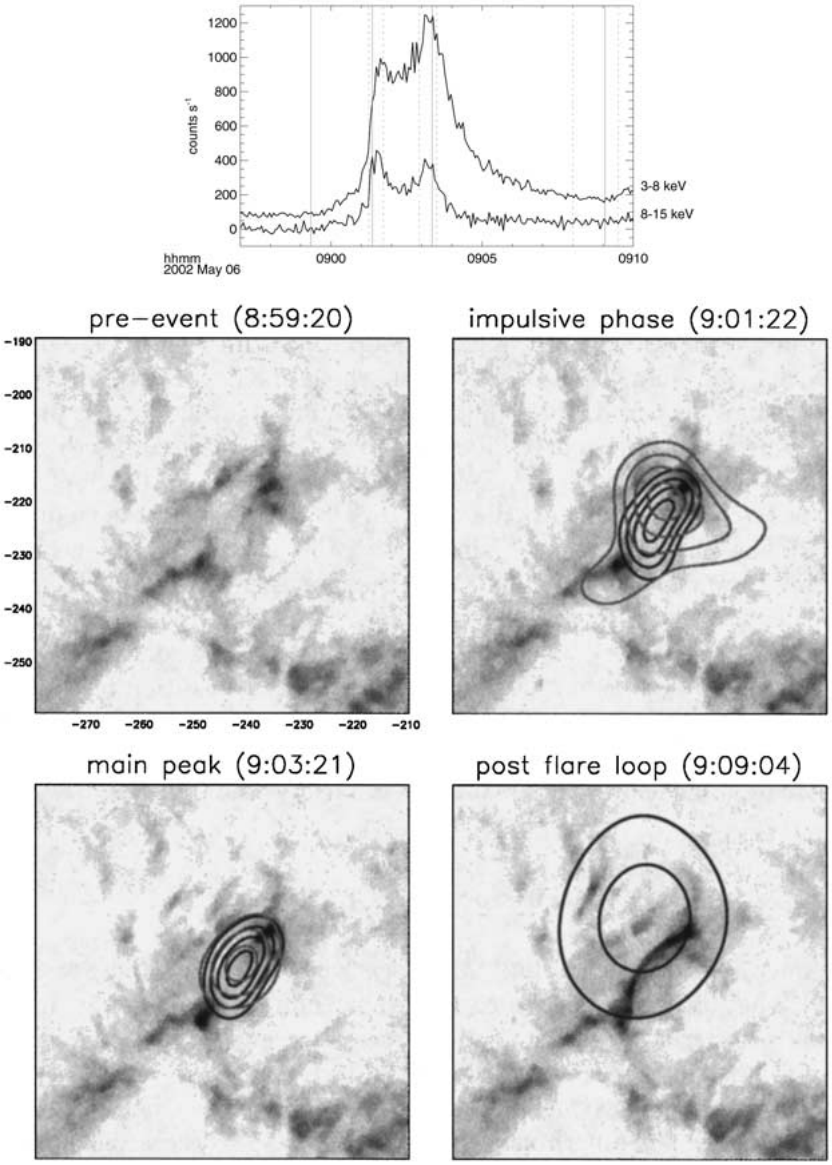

Figure 6. (a) *Top panel*: RHESSI time profiles below and above 8 keV are shown, with the integration times of the RHESSI images given by *dashed gray lines*; the *solid lines* give the time of the TRACE images. The time series above 8 keV is multiplied by a factor of 4 for a clearer representation. (b) *Lower panels* show RHESSI and TRACE observations of the microflare (GOES A8) occurring on 6 May, 09:01 UT. The images show TRACE 195 Å observations scaled to the maximum emission during the flare, superimposed are RHESSI X-ray contours (3–8 keV in *black*, 8–15 keV in *gray*; *white and red* in the color version on the CD-ROM). *Top left*: pre-event image. *Top right*: initial impulsive phase, note the different location of the 3–8 keV and 8–15 keV emission. *Bottom left*: image during main peak of the X-ray emission. *Bottom right*: later, a loop is seen with TRACE connecting the earlier flaring footpoints. The contours are 30, 50,70 90% except for the last time interval where only the 70 and 90% levels are shown.

ray emission seen with RHESSI at that time is extremely faint with the total flux in the source more than 100 times below the peak value. Using grids 7 (60 arc sec) and higher, the imaging shows a source slightly above the loop seen with TRACE. This is similar to what is observed with RHESSI in large flares (Gallagher *et al.*, 2002). We note here that the same region flares again just minutes after the microflare discussed here. In addition to the two flaring footpoints seen in EUV, much fainter brightenings occurring in the same active region are also observed, but their connection to the microflare is unclear and probably energetically unimportant.

4. Discussion and Conclusions

The microflares presented in this work can be interpreted as small flares: they occur in active regions, show non-thermal energy input as well as thermal heating with temperature and emission measure roughly following the relation found in flares (Feldman *et al.*, 1996). The main difference is that observed slopes of the non-thermal power-law spectra are steep with values between -5 to -8 whereas the spectra in normal flares are generally harder. These results are robust with respect to background subtraction while the thermal fit is much more sensitive and the given temperatures and emission measures are therefore preliminary. The non-thermal emission is observed to extend down to ~ 7 keV, in some microflares possibly below. Recent RHESSI observations of large flares (Gallagher *et al.*, 2002; Krucker and Lin, 2002) report that non-thermal emission is seen down to about 10 keV; below that the thermal emission dominates. Since the energy spectra are steep, the total energy in non-thermal electrons required to produce the observed emission is strongly dependent on the lower energy cutoff E_0 of the non-thermal spectrum and the power-law exponent, γ. The energy loss rate P of electrons above E_0 is given by Brown (1971) and Lin (1974; see Lin, Feffer, and Schwartz, 2001, for corrected factors):

$$P(> E_0) \sim E_0^{-(\gamma-1)}. \tag{1}$$

Hence, the knowledge of E_0 is crucial. In earlier work with observations above 20–25 keV, the cutoff energy was often set to 25 keV (e.g., Crosby, Aschwanden, and Dennis, 1993). For regular flares, the use of 25 keV instead of 10 keV introduces a factor of ~ 10. For the microflares present in this work, the factor is ~ 500, since the spectra are steeper and E_0 smaller. Hence, the correction for smaller events seems to be larger. This could possibly change the flare frequency distribution published by Crosby, Aschwanden, and Dennis (1993) and lead to a re-evaluation of microflare contribution to coronal heating.

To obtain the total energy in energetic electrons, the non-thermal fit of the spectra was averaged over the rise phase of the event. Then Equation (1) is used to get the energy loss rate. By multiplying by the duration of the rise phase, a rough approximation of the total energy in energetic electrons can be derived. This does

not include the non-thermal emission seen in the decay phase of some events. The derived total energies for the microflares discussed are between 10^{26} to 10^{27} erg.

The (instantaneous) total thermal energy content can be derived from the thermal fit using the emission measure and temperature together with a estimate of the source size from the RHESSI images. As a first approximation, only an upper limit of the source size is used taken from the images with $7''$ resolution. These estimates of the thermal energy content are extremely rough, but give energies of several times 10^{27} ergs, comparable to the derived total non-thermal electron energy. Of course, to obtain the total energy input to the thermal plasma requires an estimate of the energy losses as well.

Future RHESSI microflare observations will lead to more confidence in current fitting models and appropriate background subtraction. More accurate flare size estimates (see Schmahl and Hurford, 2002) will yield improved thermal energy estimates and a better understanding of low-count imaging will improve RHESSI's resolution for small flares.

Acknowledgements

This research is supported by NASA contract NAS 5-98033. We acknowledge the RHESSI team's outstanding effort in making this mission a success under adverse conditions.

References

Aschwanden, M. J., Tarbell, T. D., Nightingale, R. W., Schrijver, C. J., Title, A., Kankelborg, C. C., Martens, P., and Warren, H. P.: 2000, *Astrophys. J.* **535**, 1047.

Benz, A. O. and Grigis, P. C.: 2002, *Solar Phys.*, this volume.

Crosby, N. B., Aschwanden, M. J., and Dennis, B. R.: 1993, *Solar Phys.* **143**, 275.

Feldman, U., Doschek, G. A., Behring, W. E., and Phillips, K. J. H.: 1996, *Astrophys. J.* **460**, 1034.

Gallagher, P., Dennis, B. R., Krucker, S., Schwartz, R. A., and Tolbert, A. K.: 2002, *Solar Phys.*, this volume.

Hurford, G. J. *et al.*: 2002, *Solar Phys.*, this volume.

Kane, S. R. and Anderson, K. A.: 1970; *Astrophys. J.* **162**, 1003.

Krucker, S. and Lin, R. P.: 2002, *Solar Phys.*, this volume.

Lin, R. P., Schwartz, R. A., Kane, S. R., Pelling, R. M., and Hurley, K. C.: 1984, *Astrophys. J.* **283**, 421.

Lin, R. P., Feffer, P. T., and Schwartz, R. A.: 2001, *Astrophys. J.* **557**, L125.

Lin *et al.*: 2002, *Solar Phys.*, this volume.

Neupert, W. M.: 1968, *Astrophys. J.* **153**, L59.

Schmahl, E. J. and Hurford, G. J.: 2002, *Solar Phys.*, this volume.

Shimizu, T.: 1995, *Publ. Astron. Soc. Jap.* **47**, 251.

Tanaka, K., Watanabe, T., and Nitta, N.: 1984, *Astrophys. J.* **282**, 793.

van Beek, H. F., Hoyng, P., Lafleur, B., and Simnett, G. M.: 1980, *Solar Phys.* **65**, 39.